Systematic characterization of deubiquitylating enzymes for roles in maintaining genome integrity

Running title: Deubiquitylating enzymes in double-strand break repair

Ryotaro Nishi[1], Paul Wijnhoven[1], Carlos le Sage[1], Jorrit Tjeertes[1,2], Yaron Galanty[1], Josep V. Forment[1], Michael J. Clague[3], Sylvie Urbé[3] and Stephen P Jackson[1,4]

[1]The Wellcome Trust/Cancer Research UK Gurdon Institute and Department of Biochemistry, University of Cambridge, Cambridge, CB2 1QN, UK.

[2]Current affiliation: Developmental & Molecular Pathways, Novartis Institutes for Biomedical Research, Novartis Pharma AG, Postfach CH-4002 Basel

[3]Cellular & Molecular Physiology, Institute of Translational Medicine, University of Liverpool, Liverpool, L69 3BX, UK

[4]The Wellcome Trust Sanger Institute, Hinxton, UK.

Correspondence to Stephen P. Jackson: s.jackson@gurdon.cam.ac.uk

DNA double-strand breaks (DSBs) are perhaps the most toxic of all DNA lesions, with defects in the DNA damage response to DSBs being associated with various human diseases. Although it is known that DSB repair pathways are tightly regulated by ubiquitylation, we do not yet have a comprehensive understanding of how deubiquitylating enzymes (DUBs) function in DSB responses. Here, by carrying out a multi-dimensional screening strategy for human DUBs, we identify several with hitherto unknown links to DSB repair, the G2/M DNA-damage checkpoint and genome-integrity maintenance. Phylogenetic analyses reveal functional clustering within certain DUB subgroups, suggesting evolutionally conserved functions and/or related modes-of action. Furthermore, we establish that the DUB UCHL5 regulates DSB resection and repair by homologous recombination through protecting its interactor, NFRKB, from degradation. Collectively our findings extend the list of DUBs promoting the maintenance of genome integrity, and highlight their potential as therapeutic targets for cancer.

Genomic DNA in all organisms is exposed to various endogenously-generated and exogenous DNA damaging agents, including ultra-violet light, reactive oxygen species, ionizing radiation (IR) and chemotherapeutic medicines. These agents generate DNA lesions that threaten genome integrity by compromising normal DNA-based processes such as replication, transcription and cell division. To mitigate the deleterious effects of DNA lesions, specialized DNA repair mechanisms have evolved, whose loss or deregulation causes cancer and various hereditary diseases[1]. In eukaryotic cells, DNA double-strand breaks (DSBs), perhaps most toxic DNA lesions, are mainly repaired by homologous recombination (HR) or non-homologous end

joining (NHEJ)[2]. DSBs also trigger intracellular signaling processes termed the DNA-damage response (DDR), which includes cell-cycle checkpoint arrest responses. It is well known that DSB repair and associated events are tightly regulated by post-translational protein modifications. For instance, protein phosphorylation plays key roles in DSB repair and DDR signaling via the actions of protein kinases such as DNA-PK, ATM, ATR, CHK1 and CHK2[3-5]. Furthermore, it has become apparent that ubiquitylation – the covalent attachment of the 76 amino-acid residue protein, ubiquitin, to target molecules – also plays important roles in controlling DSB repair and DDR processes[6]. Ubiquitylation is a sequential enzymatic reaction mediated by E1, E2 and E3 enzymes, resulting in mono- or poly-ubiquitylation involving the use of seven lysine residues (K6, K11, K27, K29, K33, K48, and K63) on ubiquitin as well as the ubiquitin amino terminus[7]. The classical function of ubiquitylation, mainly via K48 linked chains, is to target substrates to proteasome dependent degradation. However, it is now clear that other types of poly-ubiquitylation as well as mono-ubiquitylation also play other prevalent roles through regulating protein interactions, activity and subcellular localisation[8].

In many instances, ubiquitylation is regulated by its removal through the actions of specific deubiquitylating enzymes (DUBs), some of which also play key roles in ubiquitin-precursor processing[9]. The human genome encodes 94 potential DUBs that can be divided into five subfamilies based on sequence and structural features of their catalytic domains: ubiquitin-specific proteases (USPs), ubiquitin carboxyl-terminal hydrolases (UCHs), ovarian tumor proteases (OTUs), Machado-Joseph disease enzymes (MJDs) and JAB1/MPN/MOV34 metalloenzymes (JAMMs)[10]. While various DUBs have been connected to DDR processes[11-18], an important challenge is

to achieve a more comprehensive understanding of DUB functions in this context. Here, to address this challenge, we have systematically characterized human DUBs for roles in DSB repair, the DNA-damage induced G2/M cell cycle checkpoint and the overt maintenance of genome integrity. In addition to identifying many DUBs with DDR roles, this work also lead to establish that one, UCHL5 promotes DSB end resection and HR through regulating the stability of the NFRKB protein that is a subunit of chromatin remodeling complex INO80.

RESULTS

Primary screens for DUBs promoting the DDR or the G2/M DNA-damage checkpoint

To identify DUBs with DSB-responsive roles, we carried out systematic screens employing three different techniques (Fig. 1). First, after cloning the coding regions for 71 of the 94 human DUBs into vectors to express them fused to green fluorescent protein (GFP) in human U2OS cells, we used live-cell imaging to examine each GFP-DUB fusion for recruitment to DNA damage sites generated by laser micro-irradiation, a technique commonly used to measure DSB-responses (Supplementary Table 1)[19]. In a parallel primary screen, we employed 90 short-interfering RNA (siRNA) pools to individually deplete each of the corresponding DUBs in human U2OS cells. Ensuing DUB-depleted cells and control cells were then treated with the DSB-generating reagent phleomycin, and cell extracts were analyzed by immunoblotting for canonical DSB-induced phosphorylations on CHK1 Ser-345, CHK2 Thr-68 and histone H2AFX (also known as H2AX) Ser-139 (γH2AX). In parallel, the effect of depleting all human DUBs on the G2/M DNA-damage

checkpoint was assessed by quantifying the mitotic mark, phosphorylated histone H3 Ser-10, before and after DNA damage induction by phleomycin (Fig. 1 and Fig. 2a).

This work identified 17 DUBs, whose depletion caused persistence of phosphorylated H3 Ser-10 after DNA damage induction (Fig. 2a) to a degree greater than two-times (green) or three-times (red) the standard deviation of the siRNA control. This thereby suggested these DUBs as playing roles in cell-cycle progression or G2/M checkpoint control (for identities of these DUBs, see Supplementary Table 1). We note that this aspect of our work identified several DUBs (CSN5, USP19 and USP37) that had been previously linked to the G2/M checkpoint, thereby providing validation of our screening methodology[20-23]. Moreover, our DNA-damage localisation and DDR signaling screens collectively identified 44 DUBs as candidates for affecting the DDR following DSB induction (Fig. 1 and Supplementary Table 1).

Identifying DUBs involved in DSB repair and/or genome integrity maintenance

To further examine whether the 44 DDR-DUB candidates we identified were involved in maintaining genome stability and/or DSB repair, we used siRNA pools to deplete them, then used neutral comet assays (Fig. 1 and see METHODS) to directly measure DSBs in cells that had or had not been exposed to phleomycin. Importantly, by employing siRNA-mediated depletion of BRCA1 and XRCC4, which play important roles in HR and NHEJ, respectively, we established that defects in either of these DSB repair pathways can be detected by the comet assay (Fig. 2b). This work indicated that depleting each of ten DUBs (USP44, PSMD14, USP26, MYSM1, OTUD6B, USP5, USP49, JOSD1, USPL1 and USP1) resulted in DSB induction even without exposing cells to phleomycin (Fig. 2c and Supplementary Table 1),

suggesting functions for these DUBs in replication and/or repairing endogenously generated DNA damages that can become converted to DSBs during replication. Moreover, these comet-assay screens identified 23 DUBs whose depletion resulted in a DSB repair defect greater than two times the standard deviation of the siRNA control (Fig. 2b and also see Fig. 4a). These included USP1, USP3, USP5, USP7, USP11, BAP1 and BRCC3 (BRCC36), which have previously-suggested DDR connections[11-18], thereby indicating that our screen identified DUBs with positive roles in DSB repair. On the other hand, we also found 13 DUBs that were recruited to DNA damage sites but gave only marginal DSB repair defects upon siRNA depletion, including OTUB1, a negative regulator of the UBE2N (UBC13) ubiquitin E2 enzyme[24], USP44 that is reported to antagonize RNF168 dependent ubiquitylation[25], and OTUB2 that functions in repair-pathway choice[26] (Fig. 2b, Fig. 3a, and Fig. 4a), suggesting that some of the additional DUBs we identified might be negative DDR regulators and/or be involved in repair-pathway choice. Interestingly, phylogenetic analysis of the DUBs that we identified with associations to DSB repair (Fig. 3b) or G2/M checkpoint control (Fig. 3c) revealed clustering in certain DUB subgroups (for instance in Fig. 3b, the entire UCH subclass and those containing USP5 and USP13, USP11 and USP15, or BRCC3 and CSN5). This suggests that these DUBs might have overlapping functions and/or related modes-of-action in DSB-responses.

To extend our analyses further, we selected the ten highest scoring DUBs from the DSB-repair secondary screen and assessed the impacts of their depletion with individual siRNAs in neutral comet assays (Fig. 4a, b; active individual siRNAs were deconvoluted from the siRNA pools through assessing their target DUBs by immunoblotting; data not shown). This work identified six DUBs (USP7, USP13,

USP15, USP20, CSN5 and UCHL5) whose depletion yielded significant and reproducible DSB repair defects in neutral comet assays (Fig. 4b). Moreover, we carried out clonogenic survival assays to establish the effect of depleting these DUBs on cellular sensitivity to ionizing radiation (IR). This revealed that depletion of each of these DUBs resulted in significant IR hypersensitivity, demonstrating that our screen effectively identified DUBs with positive roles in DSB repair (Fig. 4a-c and Fig. 5a; note that USP11 depletion, which we had found to result in a DSB repair defect in the comet assay, also caused mild IR hypersensitivity, consistent with a previous report linking it to the DDR[17]). Although it will be worthwhile pursuing DDR functions for all of these DUBs as well as others identified as putative DDR regulators by our screens, we focused our further analyses on UCHL5 (ubiquitin carboxyl-terminal hydrolase L5; also known as UCH37). This protein was prioritized because it was the only DUB other than the deneddylase CSN5 that was positive in all three of our screening assays (localisation, DDR signaling and DSB repair) and because we found that depleting each member of human UCH DUB family resulted in DSB repair defects (Fig. 3b and Fig. 4a).

UCHL5 promotes HR and extensive DNA-end resection

As shown in Figure 5a, we found that UCHL5 depletion rendered cells hypersensitive to IR in clonogenic survival assays, producing similar sensitivity as that caused by depleting BRCA1, a well-characterized HR factor. On further investigation, we observed no effect of UCHL5 depletion on NHEJ as assessed by random plasmid integration (Fig. 5b). By contrast, depleting UCHL5 with three distinct siRNAs lead to significant impairments in HR repair efficiencies as measured by a chromosomal DSB-induced gene-conversion assay system (Fig. 5c; as shown in Supplementary Fig.

1a, this was not associated with potentially confounding changes in cell-cycle profiles). Furthermore, in accordance with an HR defect, depletion of UCHL5 resulted in hypersensitivity to camptothecin, which stabilizes topoisomerase I cleavage-complexes, leading to DNA replication-dependent DSBs in S-phase that are repaired by HR-mediated mechanisms (Supplementary Fig. 1b). To determine whether these defects were indeed due to UCHL5 depletion, we established stable cell lines expressing GFP alone or GFP-tagged UCHL5 (GFP-UCHL5; Supplementary Fig. 1c). These cells were treated with a control siRNA, an siRNA targeting both endogenous UCHL5 and the GFP-UCHL5 construct, or an siRNA against the UCHL5 3' untranslated region (3'-UTR) to target endogenous UCHL5 but not GFP-UCHL5 (Fig. 5d). Importantly, the effects of endogenous UCHL5 depletion on phleomycin-induced DSB repair were rescued by expressing GFP-UCHL5 wild-type (WT) but not by expressing a GFP-UCHL5 construct (deubiquitylase dead; DD)[27] lacking deubiquitylase activity because Cys-88 was replaced by Ala (Fig. 5d and Supplementary Fig. 1c). This was despite GFP-UCHL5 DD being recruited to sites of damage as efficiently as GFP-UCHL5 WT (Fig. 5e). Taken together, these data supported a model in which UCHL5 is recruited to sites of DNA damage, where its deubiquitylase activity then promotes DSB repair.

To gain insights into how UCHL5 promotes DSB repair, we examined the effect of its depletion on DDR signaling following camptothecin treatment. This revealed that UCHL5 depletion impaired phosphorylation of replication protein A subunit 2 (RPA2) on Ser4/Ser8 (Fig. 6a). Since RPA2 Ser4/Ser8 phosphorylation defects correlate with compromised DNA-end resection[28,29], we assessed single-stranded DNA (ssDNA) production after camptothecin treatment. This revealed that ssDNA

focus formation was reduced, although still detectable, upon UCHL5 depletion (Supplementary Fig. 1d). To quantify ssDNA formation, we established a flow-cytometry based method to measure the signal intensity of native anti-BrdU staining in cells after camptothecin treatment (see METHODS). Thus, we found that UCHL5 depletion reduced resection of camptothecin-induced DSBs to a similar extent as that caused by depleting the end-resection factors EXO1 or BLM (Fig. 6b). Furthermore, while UCHL5 depletion did not abolish camptothecin-induced RPA focus production (Supplementary Fig. 1e, f), the intensities of RPA on ssDNA were reduced (Fig. 6c). UCHL5 depletion also reduced camptothecin-induced focus formation by the key HR factor RAD51, a phenotype rescued by wild-type UCHL5 but not by catalytically inactive UCHL5 (Supplementary Fig. 1g and data not shown). Furthermore, the camptothecin-induced RPA2 phosphorylation defect caused by UCHL5 depletion was rescued by wild-type but not catalytically inactive UCHL5 (Fig. 6d, e). Collectively, these data suggested that UCHL5 is dispensable for initiation of DNA-end resection but is important for the full resection process.

To define which step(s) leading to DNA-end resection was affected by UCHL5, we examined the DNA-damage recruitment of various factors linked to resection. Although, depleting UCHL5 had no marked effect on GFP-CtIP accumulation at damage sites (Fig. 6f and Supplementary Fig. 1h), it significantly impaired GFP-EXO1 recruitment (Fig. 6g). These observations implied that UCHL5 functions prior to EXO1 but after CtIP to promote resection and ensuing HR. To examine whether UCHL5 regulates extensive resection pathways involving BLM and possibly DNA2, we carried out assays in cells depleted for various resection factors. Since additive effects were observed when UCHL5 was co-depleted with either EXO1 or BLM

(Supplementary Fig. 1i), this suggested that UCHL5 affects both EXO1- and BLM-dependent resection processes.

UCHL5 affects HR repair apart from its function as a proteasome component

Because UCHL5 is a subunit of the proteasome 19S regulatory particle lid[27,30-32], and since proteasome inhibition causes defective DSB-induced RPA2 phosphorylation[33,34], we considered whether UCHL5 depletion might affect resection and HR via causing general proteasome dysfunction. However, we found that while treating cells with the proteasome inhibitor MG132 resulted in significant accumulation of ubiquitylated proteins, this did not occur upon UCHL5 depletion (Supplementary Fig. 2a). Moreover, although 53BP1 focus formation after IR was inhibited by MG132 treatment or depletion of the DDR ubiquitin E3 ligase RNF8[35-37], it was not affected by UCHL5 depletion (Supplementary Fig. 2b). Furthermore, although MG132 treatment strongly inhibited camptothecin-induced DNA-end resection (Supplementary Fig. 2c), depletion of hRPN13 (ADRM1), which recruits UCHL5 to the proteasome and enhances *in vitro* UCHL5 deubiquitylating activity[27], had only marginal effects on resection and accumulation of ubiquitylated proteins (Supplementary Fig. 2d,e), suggesting that the role of UCHL5 in resection is distinct from its proteasomal function[30,31]. While these findings did not exclude a possible DSB repair function of UCHL5 in association with the proteasome, they suggested that UCHL5 might affect resection and HR through additional mechanisms.

UCHL5 aids resection by protecting NFRKB from proteasomal degradation

Previous work has established that UCHL5 is a component of both the proteasome and the INO80 chromatin remodeling complex; these complexes being mediated via

UCHL5 interactions with hRPN13 and NFRKB (nuclear factor related to κB-binding protein), respectively (Supplementary Fig. 3a)[30,31,38]. We found that UCHL5 depletion reduced the steady-state level of NFRKB but not hRPN13 (Fig. 7a and data not shown); and time-course studies in cells treated with cycloheximide, to prevent *de novo* protein synthesis, revealed that UCHL5 depletion reduced NFRKB protein half-life (Fig. 7b). UCHL5 depletion did not, however, reduce NFRKB mRNA levels, nor protein levels of other INO80-complex subunits with suggested roles in DSB repair (Supplementary Fig. 3b, c)[39-42]. Furthermore, NFRKB reduction caused by UCHL5 depletion was rescued in cells expressing GFP-UCHL5 and was prevented by MG132 treatment (Fig. 7c and Supplementary Fig. 3d). During these studies, we observed that when cells were incubated with MG132, NFRKB in the chromatin fraction was modified in a manner enhanced by UCHL5 depletion, suggestive of ubiquitylation (Supplementary Fig. 3d). In addition, immunoprecipitation and western blotting studies established that GFP-NFRKB but not GFP alone was conjugated with ubiquitin moieties in the chromatin fraction (Fig. 7d; for controls, see Supplementary Fig. 3e, f). Also, we found that purified UCHL5 could act to remove ubiquitylations on NFRKB and/or associated proteins *in vitro* (Supplementary Fig. 3g). Taken together, these findings suggested that UCHL5 removes ubiquitin chains to protect NFRKB from proteasomal degradation.

Consistent with a model in which the effects of UCHL5 on DSB repair reflect it stabilizing NFRKB, we found that, as with UCHL5 depletion, NFRKB depletion reduced DNA-end resection in a manner complemented by a GFP-NFRKB expression construct that was resistant to a 3'UTR-targeting siRNA (Fig. 7e and Supplementary Fig. 4a). In addition, as observed for UCHL5 depletion, NFRKB depletion reduced

the intensity but not the proportion of cells with camptothecin-induced RPA foci (Supplementary Fig. 4b-d). Furthermore, NFRKB depletion decreased HR efficiency in cells as examined by a modified "traffic light reporter system" (see METHODS), RAD51 focus formation, IR resistance and camptothecin-induced RPA2 Ser4/Ser8 phosphorylation (Fig. 7f, g and Supplementary Fig. 4e, f), without markedly affecting cell cycle profiles or levels of the HR proteins XRCC3 and RAD54B[41] (Supplementary Fig. 4g, h). In accord with these findings, co-depleting NFRKB and UCHL5 had similar effects on resection as their individual depletions (Fig. 7h and Supplementary Fig. 4i). Importantly, we found that depleting INO80 chromatin remodeling complex core subunits INO80, YY1 or RUVBL1 (which are responsible for *in vitro* nucleosome remodeling activity of the complex[43]) also resulted in defective resection, HR repair efficiency, IR resistance and RPA2 phosphorylation (Fig. 7i, f, g and Supplementary Fig. 4j). Also, we found that NFRKB depletion or YY1 depletion reduced the recruitment of EXO1 to DNA damage sites, but had no discernible effect on GFP-CtIP recruitment (Supplementary Fig. 4k and data not shown). These findings therefore suggested that NFRKB contributes to DNA-end resection as a part of the INO80 chromatin remodeling complex, and support a model in which the functions of UCHL5 in DSB resection and repair are specifically connected to its role in stabilizing NFRKB. During the course of our studies, we observed that NFRKB protein levels were reduced somewhat upon camptothecin treatment, in a manner that was largely prevented by proteasome inhibition (Fig. 7j), suggesting that although it promotes resection and HR (Fig. 7e, f), NFRKB may undergo proteasome-dependent degradation/turnover after DSB induction. Interestingly, immunoprecipitation studies from MG132-treated cells revealed that NFRKB interacted with UCHL5 less in the chromatin fraction than in the

nucleoplasm, despite its interactions with INO80 being essentially equivalent in these two fractions (Fig. 7k; for input fractions, see Supplementary Fig. 4l). Collectively, these results suggested that ubiquitylation and degradation/turnover of NFRKB are regulated by dynamic, chromatin-compartment specific interactions with UCHL5 that are affected by DNA-damage induction, perhaps as a mechanism to prevent excessive ssDNA formation at DNA damage sites.

DISCUSSION

Through carrying out focused, multi-faceted systematic functional screening, we have identified DUBs that are recruited to or excluded from DNA-damage regions, as well as DUBs whose depletion affects G2/M checkpoint control, DSB induction, DSB repair and/or DSB-induced DDR signaling. In addition to identifying DUBs with already-established links to DDR processes, our findings have indicated DDR functions for DUBs that had not hitherto been connected to such events. This work thus provides a resource that will be of value in future studies to define DDR and potentially other functions for DUBs and their targets. Highlighting this potential, by studying one DUB arising from our screens, UCHL5, we have established that it functions to modulate the stability of the NFRKB component of the INO80 complex to promote HR through enhancing the key process of DNA-end resection, downstream of CtIP and at the level of EXO1 recruitment. While an involvement of the INO80 complex in DSB repair has been reported in yeast[44], and although studies in mammalian cells have connected the INO80 complex to resection[39,40,42,45], it was not known how this occurs and whether the INO80 complex directly contributes to resection rather than affecting this indirectly through its roles in transcription. We have revealed that UCHL5 and NFRKB, non-essential for the *in vitro* nucleosome

sliding activity of the INO80 complex[43] and not conserved in yeast, enhance resection by regulating the recruitment of the resection factor EXO1. This suggests that UCHL5 and NFRKB have acquired INO80-related functions in higher eukaryotes to promote and control resection in the context of higher-order chromatin or other chromatin features distinct from those found in simpler organisms. It will therefore be worthwhile exploring whether UCHL5 and INO80 control resection and HR in more compact regions of chromatin that may be recalcitrant to HR processes[46]. Given that UCHL5 depletion also resulted in moderately reduced phosphorylation of γH2AX in addition to CHK1 in our immunoblotting screens, it will also be interesting to investigate whether UCHL5 and the INO80 complex have roles in the DDR in addition to their HR-related functions. Finally, we note that developing small-molecule inhibitors of UCHL5, or other DUBs highlighted by our screens as having DDR functions, might provide opportunities for therapeutic targeting of cancers exhibiting high levels of DNA damage or which have underlying defects in DDR processes or chromatin components.

METHODS

Methods and any associated references are available in the online version of the paper.

Note: Supplementary Information is available in the online version of the paper.

Acknowledgements

We thank all members of the SPJ laboratory for helpful discussions. We are grateful to Andrew Blackford, Delphine Larrieu and Kate Dry for commenting on the manuscript, Nicola Lawrence and Alex Sossick for help with microscopy, and

Catherine Green for scientific advice. Research in the SPJ laboratory is funded by Cancer Research UK program grant C6/A11224, the European Research Council, and the European Community Seventh Framework Program grant agreement no. HEALTH-F2-2010-259893 (DDResponse). Core infrastructure funding was provided by Cancer Research UK grant C6946/A14492 and Wellcome Trust grant WT092096. SPJ receives salary from the University of Cambridge, supplemented by Cancer Research UK. RN was funded by Daiichi Sankyo Foundation of Life Science fellowship and Cancer Research UK project grant C6/A14831, ClS was funded by European Molecular Biology Organization grant ALTF 1165-2010. JF was supported by Cancer Research UK program grant C6/A11224 and the Ataxia Telangiectasia Society.

Author contributions

RN designed experiments through discussion with PW, JT, CS, YG and SPJ. PW, RN, MC and SU cloned human DUBs. RN, PW, CS and JT carried out the screens. PW and CS performed cell cycle analyses. RN performed the most of the other studies with PW's assistance. RN and SPJ wrote the paper. All other authors, especially PW, commented and suggested revisions for the paper.

Author information

Reprints and permissions information is available at www.nature.com/reprints. Readers are welcome to comment on the online version of the paper. Correspondence and requests for materials should be addressed to S.P.J. (s.jackson@gurdon.cam.ac.uk).

COMPETING FINANCIAL INTERESTS

The authors declare no competing financial interests, although SPJ points out that he is a founder and shareholder of *MISSION* Therapeutics Ltd., which is developing DUB inhibitors for therapeutic applications.

References

1 Hoeijmakers, J. H. Genome maintenance mechanisms for preventing cancer. *Nature* **411**, 366-374 (2001).

2 Khanna, K. K. & Jackson, S. P. DNA double-strand breaks: signaling, repair and the cancer connection. *Nat Genet* **27**, 247-254 (2001).

3 Kastan, M. B. DNA damage responses: mechanisms and roles in human disease: 2007 G.H.A. Clowes Memorial Award Lecture. *Mol Cancer Res* **6**, 517-524 (2008).

4 Shiloh, Y. The ATM-mediated DNA-damage response: taking shape. *Trends Biochem Sci* **31**, 402-410 (2006).

5 Jackson, S. P. Sensing and repairing DNA double-strand breaks. *Carcinogenesis* **23**, 687-696 (2002).

6 Jackson, S. P. & Durocher, D. Regulation of DNA damage responses by ubiquitin and SUMO. *Mol Cell* **49**, 795-807 (2013).

7 Kerscher, O., Felberbaum, R. & Hochstrasser, M. Modification of proteins by ubiquitin and ubiquitin-like proteins. *Annual review of cell and developmental biology* **22**, 159-180 (2006).

8 Komander, D. & Rape, M. The ubiquitin code. *Annu Rev Biochem* **81**, 203-229 (2012).

9 Reyes-Turcu, F. E., Ventii, K. H. & Wilkinson, K. D. Regulation and cellular roles of ubiquitin-specific deubiquitinating enzymes. *Annu Rev Biochem* **78**, 363-397 (2009).

10 Komander, D., Clague, M. J. & Urbe, S. Breaking the chains: structure and function of the deubiquitinases. *Nat Rev Mol Cell Biol* **10**, 550-563 (2009).

11 Khoronenkova, S. V. *et al.* ATM-dependent downregulation of USP7/HAUSP by PPM1G activates p53 response to DNA damage. *Mol Cell* **45**, 801-813 (2012).

12 Nakajima, S. *et al.* Ubiquitin-specific protease 5 is required for the efficient repair of DNA double-strand breaks. *PLoS One* **9**, e84899 (2014).

13 Nicassio, F. *et al.* Human USP3 is a chromatin modifier required for S phase progression and genome stability. *Curr Biol* **17**, 1972-1977 (2007).

14 Nijman, S. M. *et al.* The deubiquitinating enzyme USP1 regulates the Fanconi anemia pathway. *Mol Cell* **17**, 331-339 (2005).

15 Nishikawa, H. *et al.* BRCA1-associated protein 1 interferes with BRCA1/BARD1 RING heterodimer activity. *Cancer Res* **69**, 111-119 (2009).

16 Sobhian, B. *et al.* RAP80 targets BRCA1 to specific ubiquitin structures at DNA damage sites. *Science* **316**, 1198-1202 (2007).
17 Wiltshire, T. D. *et al.* Sensitivity to poly(ADP-ribose) polymerase (PARP) inhibition identifies ubiquitin-specific peptidase 11 (USP11) as a regulator of DNA double-strand break repair. *J Biol Chem* **285**, 14565-14571 (2010).
18 Yu, H. *et al.* Tumor suppressor and deubiquitinase BAP1 promotes DNA double-strand break repair. *Proc Natl Acad Sci U S A* **111**, 285-290 (2014).
19 Polo, S. E. & Jackson, S. P. Dynamics of DNA damage response proteins at DNA breaks: a focus on protein modifications. *Genes Dev* **25**, 409-433 (2011).
20 Yoshida, A., Yoneda-Kato, N. & Kato, J. Y. CSN5 specifically interacts with CDK2 and controls senescence in a cytoplasmic cyclin E-mediated manner. *Sci Rep* **3**, 1054 (2013).
21 Burrows, A. C., Prokop, J. & Summers, M. K. Skp1-Cul1-F-box ubiquitin ligase (SCF(betaTrCP))-mediated destruction of the ubiquitin-specific protease USP37 during G2-phase promotes mitotic entry. *J Biol Chem* **287**, 39021-39029 (2012).
22 Aressy, B. *et al.* A screen for deubiquitinating enzymes involved in the G(2)/M checkpoint identifies USP50 as a regulator of HSP90-dependent Wee1 stability. *Cell Cycle* **9**, 3815-3822 (2010).
23 Matsuoka, S. *et al.* ATM and ATR substrate analysis reveals extensive protein networks responsive to DNA damage. *Science* **316**, 1160-1166 (2007).
24 Nakada, S. *et al.* Non-canonical inhibition of DNA damage-dependent ubiquitination by OTUB1. *Nature* **466**, 941-946 (2010).
25 Mosbech, A., Lukas, C., Bekker-Jensen, S. & Mailand, N. The deubiquitylating enzyme USP44 counteracts the DNA double-strand break response mediated by the RNF8 and RNF168 ubiquitin ligases. *J Biol Chem* **288**, 16579-16587 (2013).
26 Kato, K. *et al.* Fine-tuning of DNA damage-dependent ubiquitination by OTUB2 supports the DNA repair pathway choice. *Mol Cell* **53**, 617-630 (2014).
27 Yao, T. *et al.* Proteasome recruitment and activation of the Uch37 deubiquitinating enzyme by Adrm1. *Nat Cell Biol* **8**, 994-1002 (2006).
28 Sartori, A. A. *et al.* Human CtIP promotes DNA end resection. *Nature* **450**, 509-514 (2007).
29 Gravel, S., Chapman, J. R., Magill, C. & Jackson, S. P. DNA helicases Sgs1 and BLM promote DNA double-strand break resection. *Genes Dev* **22**, 2767-2772 (2008).
30 Qiu, X. B. *et al.* hRpn13/ADRM1/GP110 is a novel proteasome subunit that binds the deubiquitinating enzyme, UCH37. *EMBO J* **25**, 5742-5753 (2006).
31 Hamazaki, J. *et al.* A novel proteasome interacting protein recruits the deubiquitinating enzyme UCH37 to 26S proteasomes. *EMBO J* **25**, 4524-4536 (2006).
32 Lam, Y. A., Xu, W., DeMartino, G. N. & Cohen, R. E. Editing of ubiquitin conjugates by an isopeptidase in the 26S proteasome. *Nature* **385**, 737-740 (1997).

33 Jacquemont, C. & Taniguchi, T. Proteasome function is required for DNA damage response and fanconi anemia pathway activation. *Cancer Res* **67**, 7395-7405 (2007).
34 Murakawa, Y. *et al.* Inhibitors of the proteasome suppress homologous DNA recombination in mammalian cells. *Cancer Res* **67**, 8536-8543 (2007).
35 Mailand, N. *et al.* RNF8 ubiquitylates histones at DNA double-strand breaks and promotes assembly of repair proteins. *Cell* **131**, 887-900 (2007).
36 Kolas, N. K. *et al.* Orchestration of the DNA-damage response by the RNF8 ubiquitin ligase. *Science* **318**, 1637-1640 (2007).
37 Huen, M. S. *et al.* RNF8 transduces the DNA-damage signal via histone ubiquitylation and checkpoint protein assembly. *Cell* **131**, 901-914 (2007).
38 Yao, T. *et al.* Distinct modes of regulation of the Uch37 deubiquitinating enzyme in the proteasome and in the Ino80 chromatin-remodeling complex. *Mol Cell* **31**, 909-917 (2008).
39 Gospodinov, A., Tsaneva, I. & Anachkova, B. RAD51 foci formation in response to DNA damage is modulated by TIP49. *Int J Biochem Cell Biol* **41**, 925-933 (2009).
40 Gospodinov, A. *et al.* Mammalian Ino80 mediates double-strand break repair through its role in DNA end strand resection. *Mol Cell Biol* **31**, 4735-4745 (2011).
41 Park, E. J., Hur, S. K. & Kwon, J. Human INO80 chromatin-remodelling complex contributes to DNA double-strand break repair via the expression of Rad54B and XRCC3 genes. *Biochem J* **431**, 179-187 (2010).
42 Wu, S. *et al.* A YY1-INO80 complex regulates genomic stability through homologous recombination-based repair. *Nat Struct Mol Biol* **14**, 1165-1172 (2007).
43 Chen, L. *et al.* Subunit organization of the human INO80 chromatin remodeling complex: an evolutionarily conserved core complex catalyzes ATP-dependent nucleosome remodeling. *J Biol Chem* **286**, 11283-11289 (2011).
44 Seeber, A., Hauer, M. & Gasser, S. M. Nucleosome remodelers in double-strand break repair. *Curr Opin Genet Dev* **23**, 174-184 (2013).
45 Min, J. N. *et al.* The mINO80 chromatin remodeling complex is required for efficient telomere replication and maintenance of genome stability. *Cell Res* **23**, 1396-1413 (2013).
46 Aymard, F. *et al.* Transcriptionally active chromatin recruits homologous recombination at DNA double-strand breaks. *Nat Struct Mol Biol* **21**, 366-374 (2014).

Figure legends

Figure 1 Screen to identify DUBs connected to DSB repair or the DNA damage G2/M checkpoint.

Schematic representation of the screen for human DUBs involved in DSB responses. In the primary screen, GFP-fused DUB constructs were transfected into cells stably expressing RFP-fused 53BP1, then localisation of GFP-DUBs to sites of DNA damage induced by laser micro-irradiation was examined. In parallel, each DUBs was depleted by siRNA pools and subjected to immunoblotting analysis for DDR or G2/M checkpoint markers. In the secondary screen, 44 DUBs obtained from the primary screen were subjected to neutral comet assay after depletion of each DUBs by siRNA pools.

Figure 2 Classification of screen results.

(a) Results of screen for DUBs involved in G2/M DNA-damage checkpoint. Ratio of signal intensity of phosphorylated histone H3 Ser-10 (H3 pS10) normalized to total histone H3 level before and after damage (phleomycin 40 μg/ml, 2 h) is plotted. Each DUB is numbered in ascending order based on the H3 pS10 level, with the names of the corresponding DUBs provided in Supplementary Table 1. Data shown is the one experiment carried out for each DUB depletion and the mean of ten experiments for siRNA control. Numbers 74-90, which are coloured with green or red, are: CSN6, STAMBP, USP6, HINL1, USP8, EIF3S3, USP52, UCHL1, CSN5, USP20, USP49a, USP19, USPL1, PSMD14, USP29, UCHL3 and USP37. **(b)** Results of DSB repair secondary screen with indicated DUB siRNAs. Repair efficiencies were determined by the tail moment ratio between 2 h after phleomycin (40 μg/ml) removal (recovery) and immediately after treatment (damaged) Data show the means of two (DUB, XRCC4 and BRCA1 depletions) or seven (siRNA control depletions) biologically independent experiments for respectively. **(a, b)** Two and three times standard deviation of siRNA control (2 x and 3 x SD, respectively) are indicated. Depletion of

XRCC4 and BRCA1 are supplied as positive controls. (c) Tail moments (arbitrary unit: AU) of cells transfected with indicated siRNAs without exogenous DNA-damage were plotted. Data show the means of two (DUB, XRCC4 and BRCA1 depletions) or seven (siRNA control) biologically independent experiments respectively. One times standard deviation of siRNA control is indicated by horizontal blue line.

Figure 3 Classification of DUBs based on localisation, DSB repair defects and phylogenetic analysis

(a) Classification of screen results based on localisation of GFP-DUBs to laser micro-irradiation sites and effects on DSB repair using siRNA pools (neutral comet assay). DUBs in bold represent DUBs with previously reported connections to the DDR. *: USP42 that was excluded from sites of DNA damage. **: not tested for localisation. **(b, c)** Phylogenetic analysis of human DUBs for **(c)** DSB repair or **(d)** G2/M checkpoint. DUBs are coloured green or red based on a degree of defect as shown in **a** and **b**. Human DUBs are classified into five subfamilies; ubiquitin-specific proteases (USPs), ubiquitin carboxyl-terminal hydrolases (UCHs), ovarian tumor proteases (OTUs), Machado-Joseph disease enzymes (MJDs) and JAB1/MPN/MOV34 metalloenzymes (JAMMs) (See main text introduction for details).

Figure 4 Verification of screen results.

(a) Three-dimensional scatter plot of screen results. Localisation to DNA damage sites is divided into three categories on the x-axis (no effect, recruited or excluded). Immunoblotting screen results were scored based on the numbers of altered phosphorylation signals (0, 1, 2 and 3). For the DSB repair assay, tail moment ratio is

plotted on the z-axis. DUBs are coloured based on comet assay DNA repair defects, as indicated by the bar on the left. **(b)** Neutral comet assays with two individual siRNAs targeting indicated DUBs. Data show the means of two (DUB depletions) or three (control siRNA) biologically independent experiments respectively. The blue line indicates two times standard deviation of siRNA control. DUBs that scored positive in all three screens are shown in blue. **(c)** Clonogenic survival assays with individual siRNAs targeting top hit DUBs from the screen. Data represent the individual results of two biologically independent experiments (solid lines and dashed lines).

Figure 5 UCHL5 promotes HR repair.

(a) Left: Clonogenic survival assays with IR. Depletions of XRCC4 (siXRCC4) and BRCA1 (siBRCA1) are positive controls. Data show the means of four biologically independent experiments. The error bars indicate standard error of means. Right: Depletion efficiency of UCHL5 with siRNAs targeting the coding sequence (#1 and #2) or 3'UTR. Tubulin is shown as a loading control. (**b, c)** U2OS cells or U2OS cells carrying a direct repeat-GFP reporter transfected with the indicated siRNAs were processed for NHEJ **(b)** or HR **(c)** repair assays; Ligase IV depletion (siLigIV) and CtIP depletion (siCtIP) are respective positive controls. Data show the means of two **(b)** or three **(c)** biologically independent experiments, respectively. p-values are indicated by asterisks (**; $p < 0.005$, ***; $p < 0.001$). The error bars indicate standard error of means. **(d)** GFP or GFP-UCHL5 (wild-type: WT or deubiquitylase dead: DD) expressing U2OS cells transfected with the indicated siRNAs were processed for neutral comet assays. Data represent the means of two biologically independent experiments. **(e)** U2OS cells stably expressing RFP-53BP1 were transiently

transfected with GFP-UCHL5 (WT or DD) and subjected to laser micro-irradiation. Images were taken before (undamaged: UD) or 15 min after irradiation (damaged: D). Localisation of endogenous UCHL5 to site of DNA damage was not examined due to lack of a suitable antibody. Arrows indicate irradiated areas. Scale bar indicates 10 μm.

Figure 6 UCHL5 contributes to resection by regulating EXO1 recruitment.

(a, b, c) Cells transfected with indicated siRNAs were treated with camptothecin (CPT, 1 μM, 1 h) then subjected to immunoblotting with indicated antibodies **(a)**, quantitative resection assay with anti-BrdU antibody (the means of three biologically independent experiments with standard errors of means, * means $p < 0.05$) **(b)**, or anti-RPA antibody (data represent the means of two biologically independent experiments) **(c)**. **(d, e)** GFP or GFP-UCHL5 (WT or DD) expressing U2OS cells transfected with indicated siRNAs were treated or mock treated with 1 μM of CPT for 1 h and analyzed by immunoblotting as indicated. **(f)** Intensity of GFP-CtIP at DNA damage sites relative to the unirradiated area was quantified 15 min after irradiation. Data show the means of three biologically independent experiments with error bars indicating standard errors of means. **(g)** Kinetics of GFP-EXO1 accumulation at DNA damage sites was assessed in cells transfected with indicated siRNAs. Signal intensity of GFP-EXO1 at DNA damage sites relative to the unirradiated area was quantified. Data show the means of three biologically independent experiments with error bars indicating standard errors of means.

Figure 7 UCHL5 regulates resection by protecting NFRKB from proteasomal degradation.

(a) Cells transfected with indicated siRNAs were processed for immunoblotting with indicated antibodies. Arrow indicates position of NFRKB. **(b)** Left: Cells transfected with indicated siRNAs were incubated with 100 μg/ml of cycloheximide (CHX) for various times and processed for immunoblotting with indicated antibodies. Right: Quantification of data shown on left. Data show the means of two biologically independent experiments. **(c)** GFP or GFP-UCHL5 expressing cells transfected with indicated siRNAs were analyzed by immunoblotting as indicated. **(d)** GFP and GFP-NFRKB expressing cells were mock transfected or transiently transfected with an expression plasmid of HA-tagged ubiquitin (HA-Ub). Chromatin fractions were immunoprecipited with an anti-GFP antibody followed by immunoblotting. Brackets indicate ubiquitylated NFRKB. For inputs, see Supplementary Fig. 3f. **(e)** GFP or GFP-NFRKB stably expressing cells transfected with indicated siRNAs were subjected to quantitative resection assays. Data show the means of two biologically independent experiments. **(f)** Modified "traffic light reporter system" based HR assay with indicated siRNAs. Data show the means of two biologically independent experiments. **(g)** U2OS cells transfected with indicated siRNAs were subjected to clonogenic survival assays after IR. Data show the means of two biologically independent experiments. **(h)** Cells transfected with individual or indicated combinations of siRNAs were processed for quantitative resection assays. Data show the means of two biologically independent experiments. **(i)** U2OS cells transfected with indicated siRNAs were subjected to quantitative resection assays. Data show the means of two biologically independent experiments. **(j)** U2OS cells were incubated with CHX (100 μg/ml) and or MG132 (10 μM) for 1 h prior to camptothecin (CPT) treatment (1 μM, 1 h). Nucleoplasmic fractions were subjected to immunoblotting with indicated antibodies. Relative protein levels of NFRKB are indicated with

normalization by HDAC1 levels. (k) After incubating GFP or GFP-NFRKB expressing cells with 10 μM MG132, nucloplasmic (Nu) and chromatin (Ch) fraction were immunoprecipitated with anti-GFP antibody followed by immunoblotting. For inputs, see Supplementary Fig. 4l.

METHODS

Cell lines and cell culture

All cell lines were cultured at 37˚C in a 5% CO_2 humidified atmosphere. U2OS cell lines stably expressing GFP[47], GFP-53BP1, RFP-53BP1[48], GFP-UCHL5 (WT and DD), GFP-NFRKB and GFP-CtIP[49] were cultured with Dulbecco's modified Eagle medium (DMEM, Sigma-Aldrich) containing 10% fetal bovine serum (FBS, Gibco), 100 U/ml penicillin (Gibco), 100 μg/ml streptomycin (Gibco), 292 μg/ml L-Glutamine (Gibco) and 500 μg/ml Geneticin (Gibco). U2OS cells were cultured with identical media without Geneticin. The stable U2OS cell line expressing both GFP-EXO1 and monomeric version of Kusabira Orange2-fused human Geminin (1-110 a. a.) (mKO2-hGeminin) [50] was cultured with the Geneticin containing media described above supplemented with 200 μg/ml Hygromycin B (Invitrogen). U2OS cells stably expressing the HR reporter Direct Repeat-GFP and U2OS cells carrying modified traffic light reporter based HR assay were cultured with DMEM containing FBS, penicillin, streptomycin, L-Glutamine and 1 μg/ml of puromycin (Sigma-Aldrich).

Live cell imaging based screening

U2OS cells stably expressing RFP-53BP1 in 35 mm glass-bottom dishes (WillCo-dish) were transfected with 1 μg of expression plasmids coding each GFP-DUB with FuGENE 6 and further cultured for 48 hours in the presence of 10 μM 5-Bromo-2'-deoxyuridine (BrdU). On the day of analysis, the media was replaced with phenol red-free DMEM (Sigma-Aldrich) supplemented with 10% FBS, penicillin, streptomycin and 25 mM HEPES buffer (pH 7.0-7.6, Sigma-Aldrich). DNA damage was induced by irradiating cells through a UPlanSApo 60 x /1.35 oil objective lens with UV-A laser (405 nm) using a IX81 confocal microscope (Olympus) equipped with a 37˚C

heating stage (Ibidi). The laser output was set at 400 μW with 50 scans of 10 msec/pixel. Up to 1 hour after damage induction, images were taken and analyzed by using FluoView 1000 software (Olympus).

Immunoblotting based screen

U2OS cells were transfected with 30 nM of siRNA control (AllStars Negative Control, QIAGEN) or an siRNA pool of four siRNAs targeting each DUB (QIAGEN) over two days using HiPerFect (QIAGEN). Seventy-two hours after the initial siRNA transfection, the cells were treated with 40 μg/ml of phleomycin for 2 hours or mock treated. After phleomycin removal, the cells were further cultured for 6 hours. For immunoblotting analysis, cell extracts were prepared with Laemmli buffer [62.5 mM Tris-HCl (pH 6.8), 10% Glycerol, 2% sodium dodecyl sulfate and 5% β-mercaptoethanol] at each time point and protein concentration of the samples was determined by measuring absorbance at 280 nm using a NanoDrop (Thermo Scientific) with bovine serum albumin protein standard (Thermo Scientific).

Neutral comet assay

Seventy-two hours after 30 nM siRNA transfection, the cells were incubated with 40 μg/ml phleomycin for 2 hours or mock incubated. Following phleomycin treatment, cells were washed twice with PBS and cultured for an additional 2 hours. The cells were subsequently washed twice with PBS (-) (Gibco) and collected by trypsinization. Approximately 5 x 10^3 cells in 10 μl of PBS (-) were mixed with 90 μl of LMAgarose (TREVIGEN), placed on GelBond Film (Lonza), covered with a 22 mm cover slide (VWR INTERNATIONAL) and left at 4˚C for 1 hour. Upon removal of the cover slide, the cells were lysed with Lysis Solution (TREVIGEN) at 4˚C for 1 hour.

Following a wash with TBE [90 mM Tris-Borate (pH 8.3) and 2 mM ethylenediaminetetraacetic acid (EDTA)], the samples were subjected to electrophoresis at 35 V, for 7 min in TBE. After washing with TBE, samples were fixed with 70% ethanol for 5 min at room temperature and dried overnight. The nuclei were stained with SYBR Green I (Invitrogen) in 10 mM Tris-HCl (pH 7.5) and 1 mM EDTA for 5 min at 4˚C. Images were taken with a fluorescent microscope IX71 (Olympus) with Cell^F software (Olympus). Tail moments were measured by using CometScore software (TriTek). The means of tail moment of at least 30 cells or 50 cells were measured per condition for screen with siRNA pools or for the assay with the individual siRNAs, respectively. Efficiency of DSB repair was determined as the tail moment ratio between 2 hours after phleomycin removal and immediately after treatment.

Clonogenic survival assay

Clonogenic viability was examined using a colony formation assay. Briefly, forty-eight hours after initial transfection with siRNAs, cells were seeded in 6 well plates and treated with acute IR or various doses of camptothecin for 1 hour on the following day. Colonies were stained with crystal violet solution [2% crystal violet (Sigma-Aldrich) in 10% ethanol] 10-13 days after DNA damaging reagent treatment.

NHEJ and HR repair assay

NHEJ and HR repair assay was carried out as previously described[51]. Briefly, NHEJ repair efficiency was examined by random plasmid integration. HR repair efficiency was investigated by a chromosomal DSB-induced gene-conversion assay system with transient expression of I-SceI restriction enzyme in U2OS cells carrying Direct-

Repeat GFP reporter as previously described or in U2OS cells carrying modified "traffic light reporter system" that was modified from the published protocol[52] (J. V. F. et al. personal communication).

Immunofluorescent staining

For the purpose of single-strand DNA detection, cells were fixed with methanol for 30 min at -20˚C and subsequently washed once with ice-cold acetone. In all the other experiments, cells were fixed with 4% paraformaldehyde for 15 min at room temperature and then permeabilized by incubating with 0.2% Triton X-100 in PBS for 5 min at room temperature. To examine RPA2 foci formation, cells were pre-extracted prior to fixation with pre-extraction buffer [10 mM Pipes (pH 6.8), 3 mM $MgCl_2$, 3 mM EDTA, 0.5% Triton X-100, 0.3 M Sucrose and 50 mM NaCl] for 5 min on ice. Hereafter, samples were washed twice with 0.1% Tween 20 in PBS after each procedure. After incubating cells with blocking buffer [5% FBS, 0.1% Triton X-100 in PBS] for 30 min, cells were sequentially incubated with primary antibodies for 1 hour and with secondary antibodies for 30 min diluted in blocking buffer. Following nuclei staining with 1 μg/ml of 4',6-diamidino-2-phenylindole (DAPI) solution for 10 min, samples were sealed with VECTASHIELD (Vector) and images were taken as described above.

Cell extract preparation

Except for the immunoblotting based screen and cellular fractionation, cell extracts were prepared with CSK buffer [10 mM PIPES (pH 6.8), 3 mM $MgCl_2$, 1 mM ethylene glycol tetraacetic acid (EGTA), 0.1% Triton X-100, 300 mM sucrose and 300 mM NaCl] containing 1 x protease inhibitor cocktail (Roche), 1 x phosphatase

inhibitor cocktail (Sigma-Aldrich), 20 mM N-Ethylmaleimide (NEM, Sigma-Aldrich) and 0.25 mM Phenylmethanesulfonyl fluoride (PMSF, Sigma-Aldrich). Cells were washed twice with ice-cold PBS and incubated with an appropriate volume of CSK buffer for 1 hour on ice with occasional mixing. Soluble fractions were collected by centrifugation at 20,000 x g for 10 min at 4˚C. The residual pellet fraction was washed twice and resuspended with the same buffer, followed by sonication. For immunoblotting based screens, after washing with ice-cold PBS, cells were lysed with Laemmli buffer and boiled for 5 min at 95˚C. For cellular fractionation, cells collected with ice-cold PBS were incubated on ice for 5 min with hypotonic buffer [10 mM HEPES (pH 7.4), 10 mM KCl, 2 mM $MgCl_2$, 340 mM sucrose, 10% glycerol and 0.1% Triton X-100] containing 1 x protease inhibitor cocktail, 1 x phosphatase inhibitor cocktail, 20 mM NEM and 0.25 mM PMSF. The cytoplasmic fraction was isolated by low speed centrifugation (1,500 x g, 5 min at 4˚C). The residual pellet was washed once with hypotonic buffer and resuspended with nuclear extraction buffer [NEB; 20 mM HEPES (pH 7.4), 2 mM $MgCl_2$, 1 mM EGTA, 25% glycerol, 0.1% Triton X-100] containing 300 mM NaCl, 1 x protease inhibitor cocktail, 1 x phosphatase inhibitor cocktail, 20 mM NEM and 0.25 mM PMSF. The nucleoplasm fraction was obtained by vortexing for 30 min at 4˚C, followed by centrifugation at 20,000 x g for 10 min. The pellet was washed, resuspended with NEB containing 0.3 M NaCl, solubilized by sonication and saved as chromatin fraction. Protein concentration of cell extracts was determined with the Coomassie Protein Assay Reagent (Thermo Scientific).

Quantitative DNA-end resection assay

For direct detection of single-stranded DNA formation in the context of DNA-end resection, cells were incubated with 30 μM of BrdU for 24 hours prior to 1 μM of camptothecin treatment for 1 hour. Following camptothecin treatment, cells were collected by trypsinization, washed twice with PBS and fixed with 70% ethanol at -20˚C overnight. Hereafter cells were washed with 0.1% Tween 20 in PBS between each procedure. After incubation with blocking buffer (5% FBS, 0.1% Triton X-100 in PBS) for 30 min, cells were incubated for 1 hour with anti-BrdU antibody and anti-Cyclin A antibody in blocking buffer under non-denaturing condition to detect only ssDNA with anti-BrdU antibody. The cells were further incubated with anti-rabbit IgG antibody conjugated with Alexa Fluor® 594 and anti-mouse IgG antibody conjugated with Alexa Fluor® 488 (Life Technology) in the dark for 30 min. The cells were suspended in 1 μg/ml of DAPI solution and processed with LSRFortessa (BD Biosciences). RPA loading onto ssDNA generated through DNA-end resection during HR was quantitatively measured as previously described by using an anti-Cyclin A antibody instead of an anti-γH2AX antibody[53]. The anti-BrdU or anti-RPA antibody signal intensities were obtained from a subpopulation of cells that was positive for anti-Cyclin A antibody staining using FlowJo software (TreeStar). After subtraction of the camptothecin non-treated background signal, the mean intensity of the anti-BrdU and anti-RPA antibody staining of each sample was normalized to that seen immediately after camptothecin treatment with siRNA control.

Immunoprecipitation

Nucleoplasm fractions, chromatin fractions or soluble fractions from cell extracts prepared with CSK buffer, were immunoprecipitated with an anti-GFP antibody coupled to agarose beads (GFP-Trap_A, ChromoTek) or anti-HA antibody coupled to

agarose beads (EZview Red Anti-HA Affinity Gel, Sigma-Aldrich) by rotating overnight at 4˚C. The beads were washed six times with their respective cell extraction buffer and bound proteins were eluted by boiling at 95˚C for 10 min with 1 x Laemmli SDS buffer [62.5 mM Tris-HCl (pH 6.8), 2% SDS, 10% Glycerol, 0.002% Bromophenol blue]. For the detection of ubiquitylated proteins, beads were washed twice with the buffer used for cell extract preparation, three times with same buffer containing 500 mM NaCl and once with the original buffer, followed by elution as described above.

Cell cycle profile analysis

U2OS cells were incubated for 30 min with 10 μM of BrdU, harvested by trypsinization and fixed with 70% ethanol overnight at -20˚C. Hereafter, the samples were washed twice with PBS containing 0.1% Tween 20. The samples were then incubated with denaturing solution (5 M HCl and 0.5% Triton X-100) at 37˚C for 20 min and neutralized with 0.1 M $Na_2B_4O_7$. After blocking buffer incubation, samples were incubated with anti-BrdU antibody and an Alexa Flour 488 conjugated secondary antibody. Finally, the samples were incubated with PI buffer [10 μg/ml propidium iodide (PI, Invitrogen), 250 μg/ml RNaseA (Invitrogen)] for 20 min at 37˚C and analyzed with LSRFortessa.

***In vivo* ubiquitylation assay**

The HA-tagged ubiquitin expression vector was transiently transfected in appropriate cell lines. Forty-eight hours after transfection, fractionated cell extracts were prepared and subjected to immunoprecipitation as described above.

In vitro deubiquitylation assay

Stable cell lines expressing GFP-NFRKB were transiently transfected with a plasmid coding HA-tagged ubiquitin and forty-eight hours after transfection 2 mg of nucleoplasm extracts were prepared as described above. GFP-NFRKB was immunoprecipitated with anti-GFP antibody conjugated beads in an identical way to that described in the immunoprecipitation section. Furthermore, the beads were washed twice with deubiquitylation buffer [50 mM (Tris-HCl, pH 7.5), 100 mM NaCl, 1 mM DTT, 0.5 mM EDTA, 1 x protease inhibitor cocktail, 1 x phosphatase inhibitor cocktail and 0.25 mM PMSF]. The deubiquitylation reaction was performed in a total volume of 50 µl deubiquitylation buffer by incubating immunoprecipitated GFP-NFRKB (approximately 125 µg/reaction) with 100 or 200 ng of recombinant GST-UCHL5 (Abnova) for 1 hour at 37˚C. The reaction was terminated by adding 12.5 µl of 4 x SDS sample buffer and subsequent boiling at 95˚C for 10 min. The supernatant was subjected to immunoblotting analysis.

RT-qPCR

Total mRNA was isolated from U2OS cells transfected with siRNAs by using RNeasy kit (QIAGEN) and residual genomic DNA was digested with TUROB-DNA free kit (Life Technologies). Total mRNAs were reverse transcribed into cDNA using SuperScript III First-Strand Synthesis System (Life Technologies) with an oligo dT primer. Quantitative PCR was performed using Fast SYBR Green master mix (Life Technologies) and StepOnePlus Real-Time PCR System (Life Technologies) with GAPDH targeting primers (5’ GTCAGCCGCATCTTCTTTTG 3’, 5’ GCGCCCAATACGACCAAATC 3’) and NFRKB targeting primers (5’ CATTGCCCGCCATTCCCATC 3’, 5’ CACCACTCGCACCTGAGACA 3’).

Live cell imaging with laser micro-irradiation

U2OS cells stably expressing GFP-CtIP or both GFP-EXO1 and mKO2-hGeminin were incubated with 10 μM of BrdU for 24 hours prior to laser micro-irradiation. For quantitative analysis of accumulation to sites of damage, cells were irradiated with reduced laser output (200 μW) to avoid excess generation of single-stranded DNA. For GFP-EXO1 accumulation kinetics, images were taken every 6 seconds up to 300 seconds after irradiation with the microscope and software as described for live cell imaging based screening (see previous section). For GFP-CtIP, images were taken 15 minutes after irradiation. Each single experiment contains at least 10 cells and in total at least 30 cells were analyzed.

Ionizing irradiation

IR was performed with the Faxitron X-ray machine (Faxitron X-ray Corporation).

Antibodies and siRNAs

Antibodies and siRNAs used in this research are summarized in Supplementary Table 2 and 3, respectively.

Statistic and quantitative analysis

All statistic analysis was done by standard student *t*-test with two-sided. For quantitative analysis, mean was used as a center value. The experiments shown with representative images were successfully reproduced at least twice.

References related to METHODS section

47 Kolas, N. K. *et al.* Orchestration of the DNA-damage response by the RNF8 ubiquitin ligase. *Science* **318**, 1637-1640 (2007).
48 Galanty, Y. *et al.* Mammalian SUMO E3-ligases PIAS1 and PIAS4 promote responses to DNA double-strand breaks. *Nature* **462**, 935-939 (2009).
49 Huertas, P. & Jackson, S. P. Human CtIP mediates cell cycle control of DNA end resection and double strand break repair. *J Biol Chem* **284**, 9558-9565 (2009).
50 Sakaue-Sawano, A. *et al.* Visualizing spatiotemporal dynamics of multicellular cell-cycle progression. *Cell* **132**, 487-498 (2008).
51 Galanty, Y., Belotserkovskaya, R., Coates, J. & Jackson, S. P. RNF4, a SUMO-targeted ubiquitin E3 ligase, promotes DNA double-strand break repair. *Genes Dev* **26**, 1179-1195 (2012).
52 Certo, M. T. *et al.* Tracking genome engineering outcome at individual DNA breakpoints. *Nat Methods* **8**, 671-676 (2011).
53 Forment, J. V., Walker, R. V. & Jackson, S. P. A high-throughput, flow cytometry-based method to quantify DNA-end resection in mammalian cells. *Cytometry A* **81**, 922-928 (2012).

Figure 1

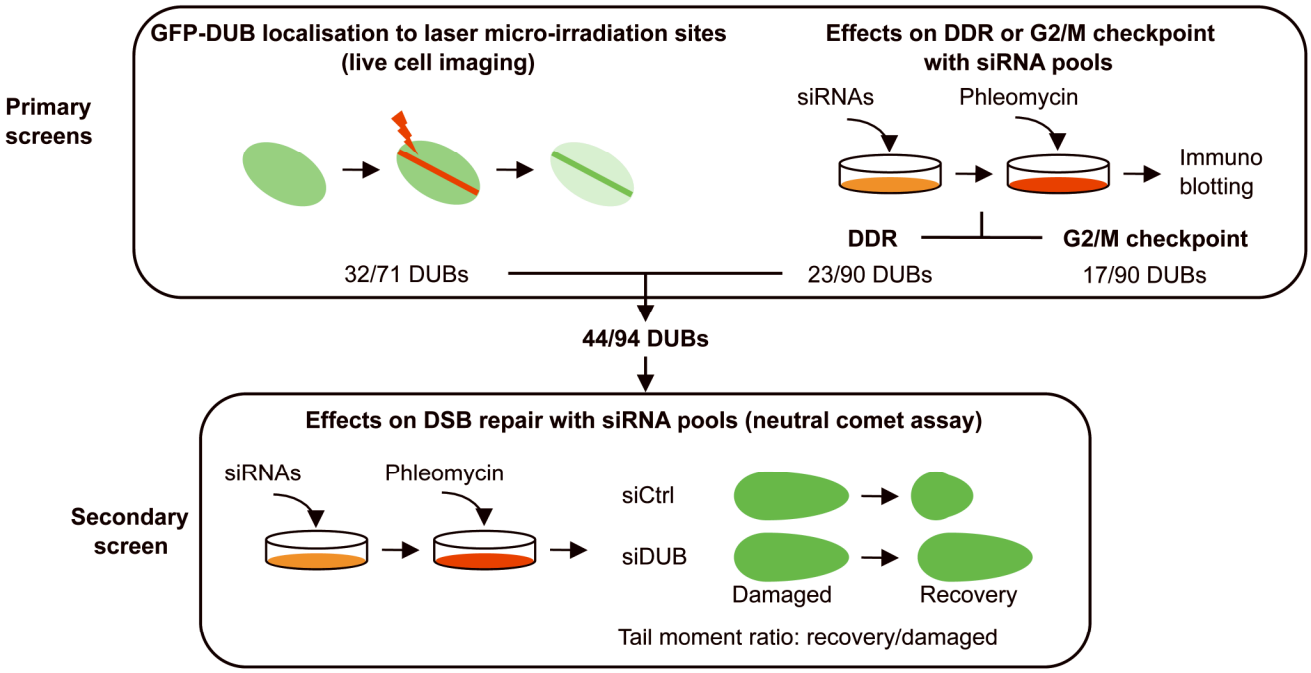
Primary screens
GFP-DUB localisation to laser micro-irradiation sites (live cell imaging)
Effects on DDR or G2/M checkpoint with siRNA pools
siRNAs
Phleomycin
Immuno blotting
DDR
G2/M checkpoint
32/71 DUBs
23/90 DUBs
17/90 DUBs
44/94 DUBs
Secondary screen
Effects on DSB repair with siRNA pools (neutral comet assay)
siRNAs
Phleomycin
siCtrl
siDUB
Damaged
Recovery
Tail moment ratio: recovery/damaged

Figure 2

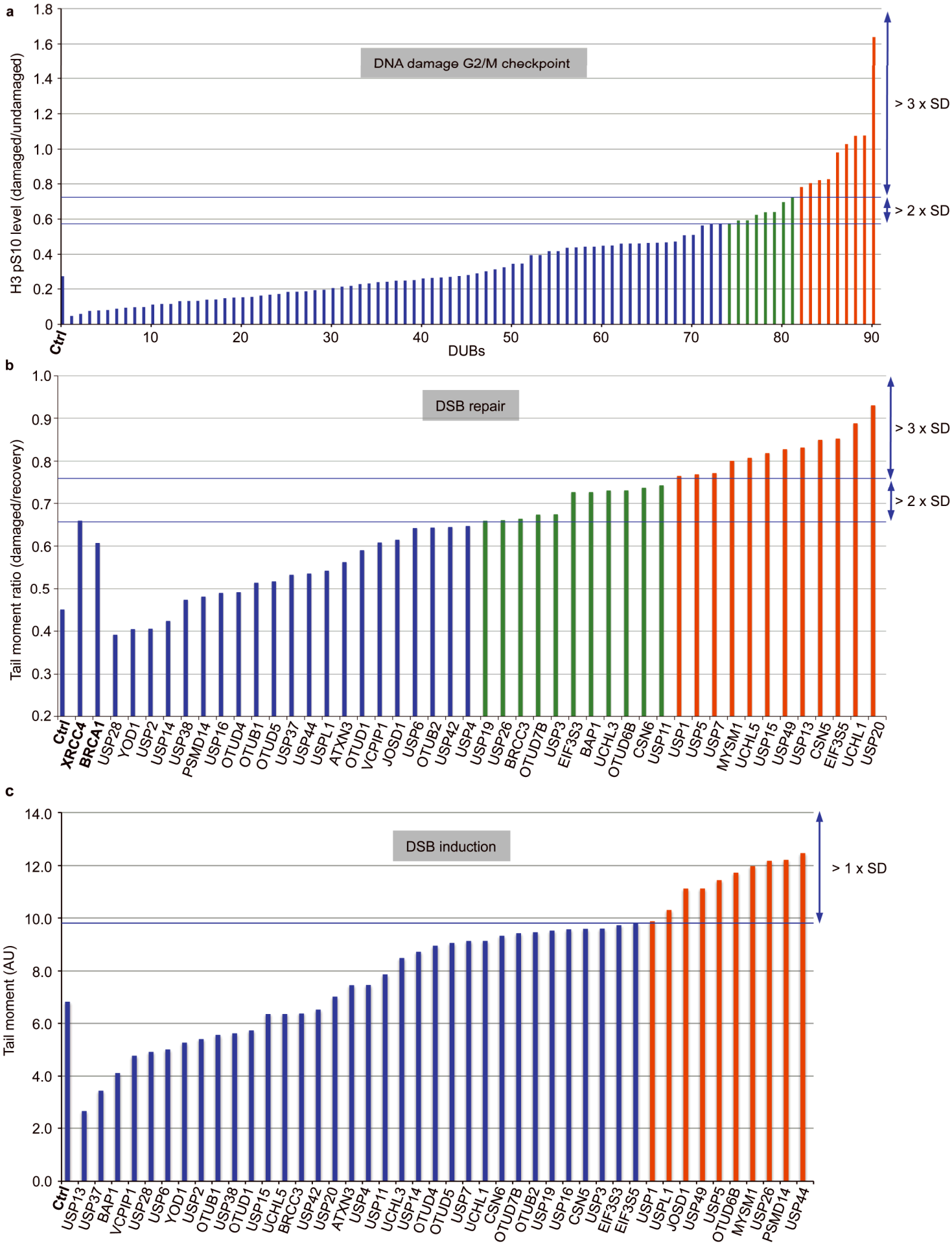
a
DNA damage G2/M checkpoint
H3 pS10 level (damaged/undamaged)
DUBs
> 3 x SD
> 2 x SD
Ctrl
b
DSB repair
Tail moment ratio (damaged/recovery)
> 3 x SD
> 2 x SD
Ctrl
XRCC4
BRCA1
USP28
YOD1
USP2
USP14
USP38
PSMD14
USP16
OTUD4
OTUB1
OTUD5
USP37
USP44
USPL1
ATXN3
OTUD1
VCPIP1
JOSD1
USP6
OTUB2
USP42
USP4
USP19
USP26
BRCC3
OTUD7B
USP3
EIF3S3
BAP1
UCHL3
OTUD6B
CSN6
USP11
USP1
USP5
USP7
MYSM1
UCHL5
USP15
USP49
USP13
CSN5
EIF3S5
UCHL1
USP20
c
DSB induction
Tail moment (AU)
> 1 x SD
Ctrl
USP13
USP37
BAP1
VCPIP1
USP28
USP6
YOD1
USP2
OTUB1
USP38
OTUD1
USP15
UCHL5
BRCC3
USP42
USP20
ATXN3
USP4
USP11
UCHL3
USP14
OTUD4
OTUD5
USP7
UCHL1
CSN6
OTUD7B
OTUB2
USP19
USP16
CSN5
USP3
EIF3S3
EIF3S5
USP1
USPL1
JOSD1
USP49
USP5
OTUD6B
MYSM1
USP26
PSMD14
USP44

Figure 3

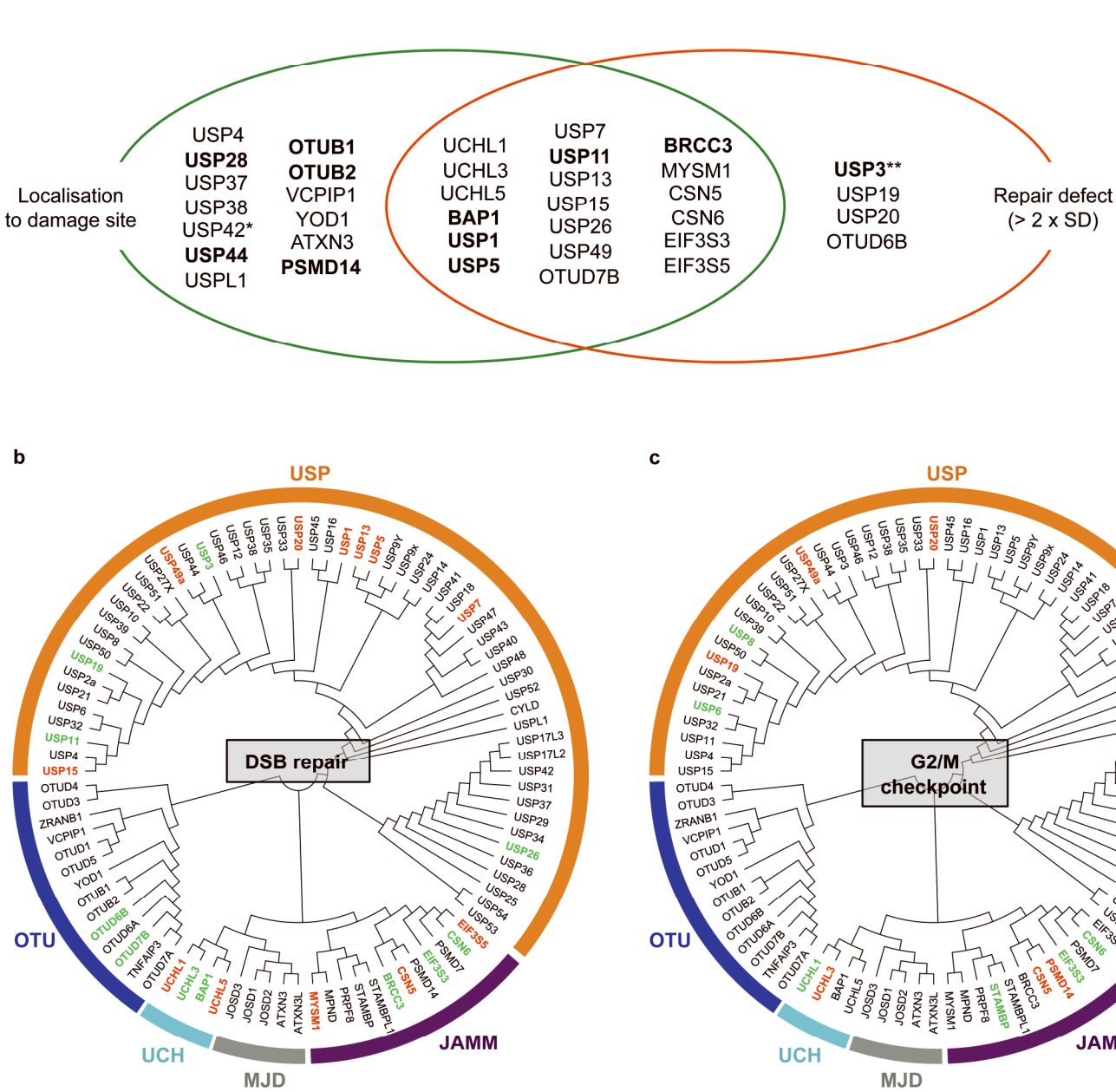
a
Localisation to damage site
USP4
USP28
USP37
USP38
USP42*
USP44
USPL1
OTUB1
OTUB2
VCPIP1
YOD1
ATXN3
PSMD14
UCHL1
UCHL3
UCHL5
BAP1
USP1
USP5
USP7
USP11
USP13
USP15
USP26
USP49
OTUD7B
BRCC3
MYSM1
CSN5
CSN6
EIF3S3
EIF3S5
USP3**
USP19
USP20
OTUD6B
Repair defect (> 2 x SD)
b
USP
OTU
UCH
MJD
JAMM
DSB repair
c
USP
OTU
UCH
MJD
JAMM
G2/M checkpoint

Figure 4

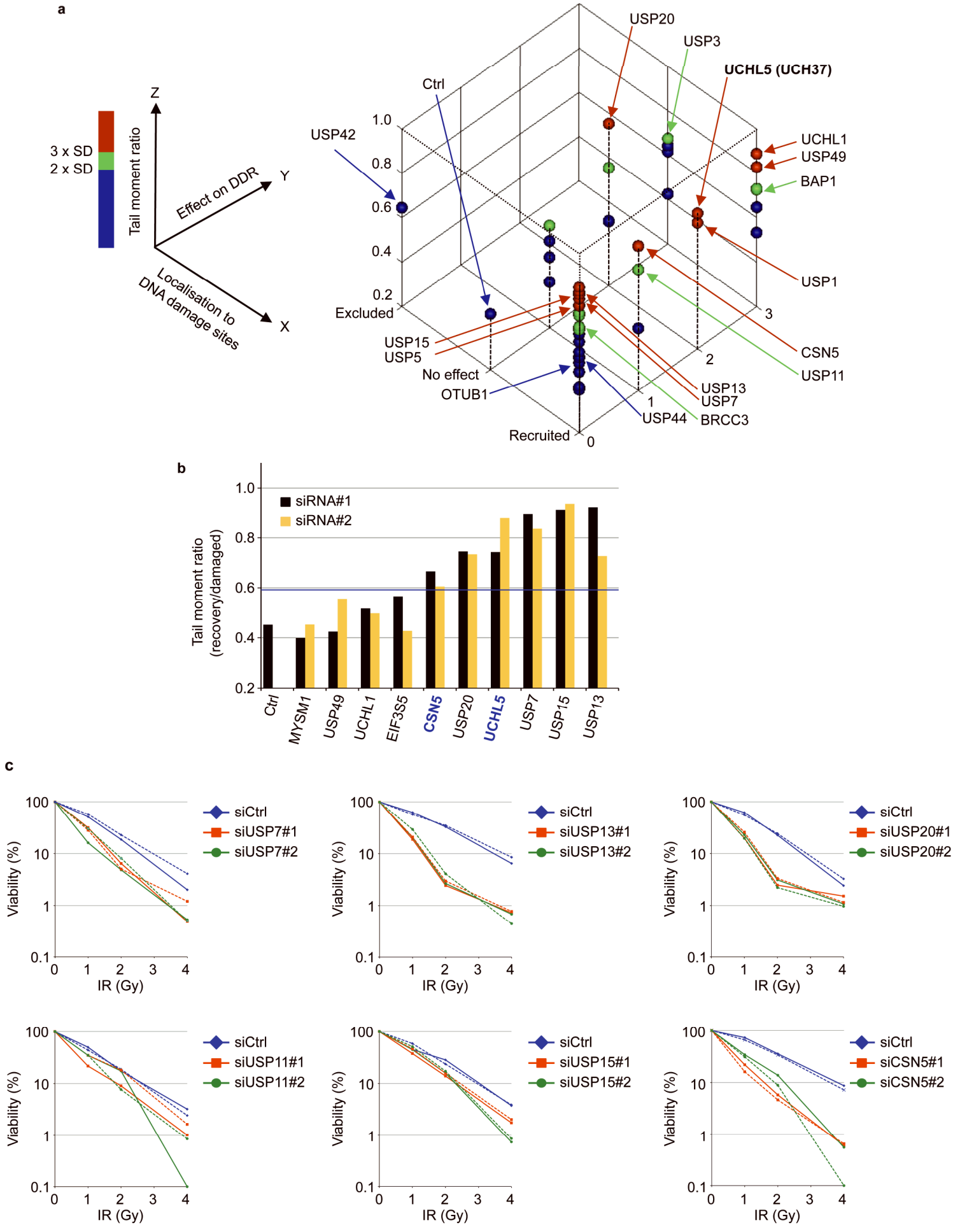
a
3 x SD
2 x SD
Tail moment ratio
Z
Effect on DDR
Y
Localisation to DNA damage sites
X
Ctrl
USP20
USP3
UCHL5 (UCH37)
USP42
UCHL1
USP49
BAP1
USP1
CSN5
USP11
USP13
USP7
USP44
BRCC3
USP15
USP5
No effect
OTUB1
Excluded
Recruited
1.0
0.8
0.6
0.4
0.2
0
1
2
3
b
siRNA#1
siRNA#2
Tail moment ratio (recovery/damaged)
Ctrl
MYSM1
USP49
UCHL1
EIF3S5
CSN5
USP20
UCHL5
USP7
USP15
USP13
c
siCtrl
siUSP7#1
siUSP7#2
siUSP13#1
siUSP13#2
siUSP20#1
siUSP20#2
siUSP11#1
siUSP11#2
siUSP15#1
siUSP15#2
siCSN5#1
siCSN5#2
Viability (%)
IR (Gy)

Figure 5

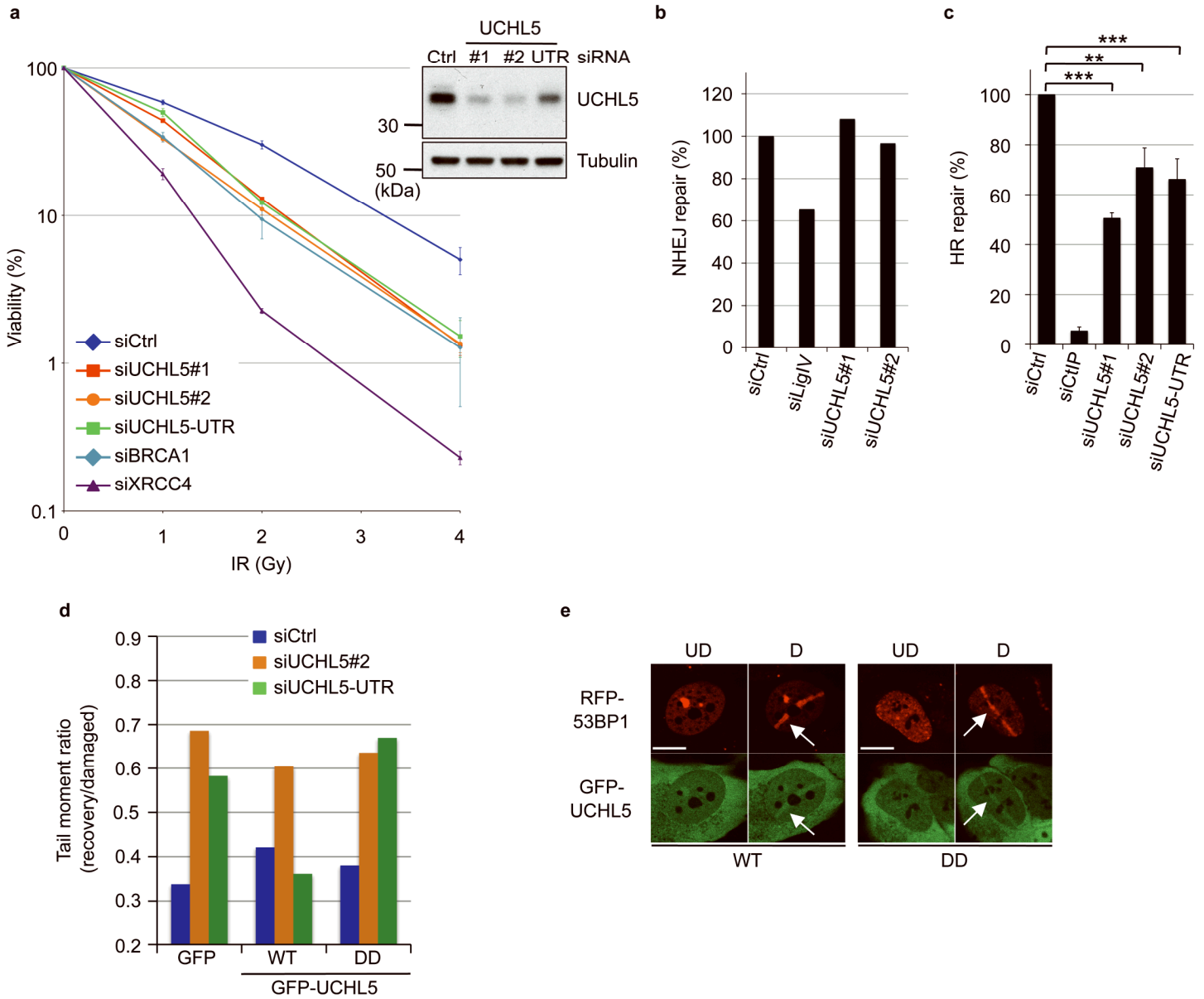
a
UCHL5
Ctrl #1 #2 UTR siRNA
UCHL5
Tubulin
30
50
(kDa)
Viability (%)
100
10
1
0.1
0
1
2
3
4
IR (Gy)
siCtrl
siUCHL5#1
siUCHL5#2
siUCHL5-UTR
siBRCA1
siXRCC4
b
NHEJ repair (%)
120
100
80
60
40
20
0
siCtrl
siLigIV
siUCHL5#1
siUCHL5#2
c
HR repair (%)
***
**
***
100
80
60
40
20
0
siCtrl
siCtIP
siUCHL5#1
siUCHL5#2
siUCHL5-UTR
d
Tail moment ratio
(recovery/damaged)
0.9
0.8
0.7
0.6
0.5
0.4
0.3
0.2
siCtrl
siUCHL5#2
siUCHL5-UTR
GFP
WT
DD
GFP-UCHL5
e
UD
D
UD
D
RFP-
53BP1
GFP-
UCHL5
WT
DD

Figure 6

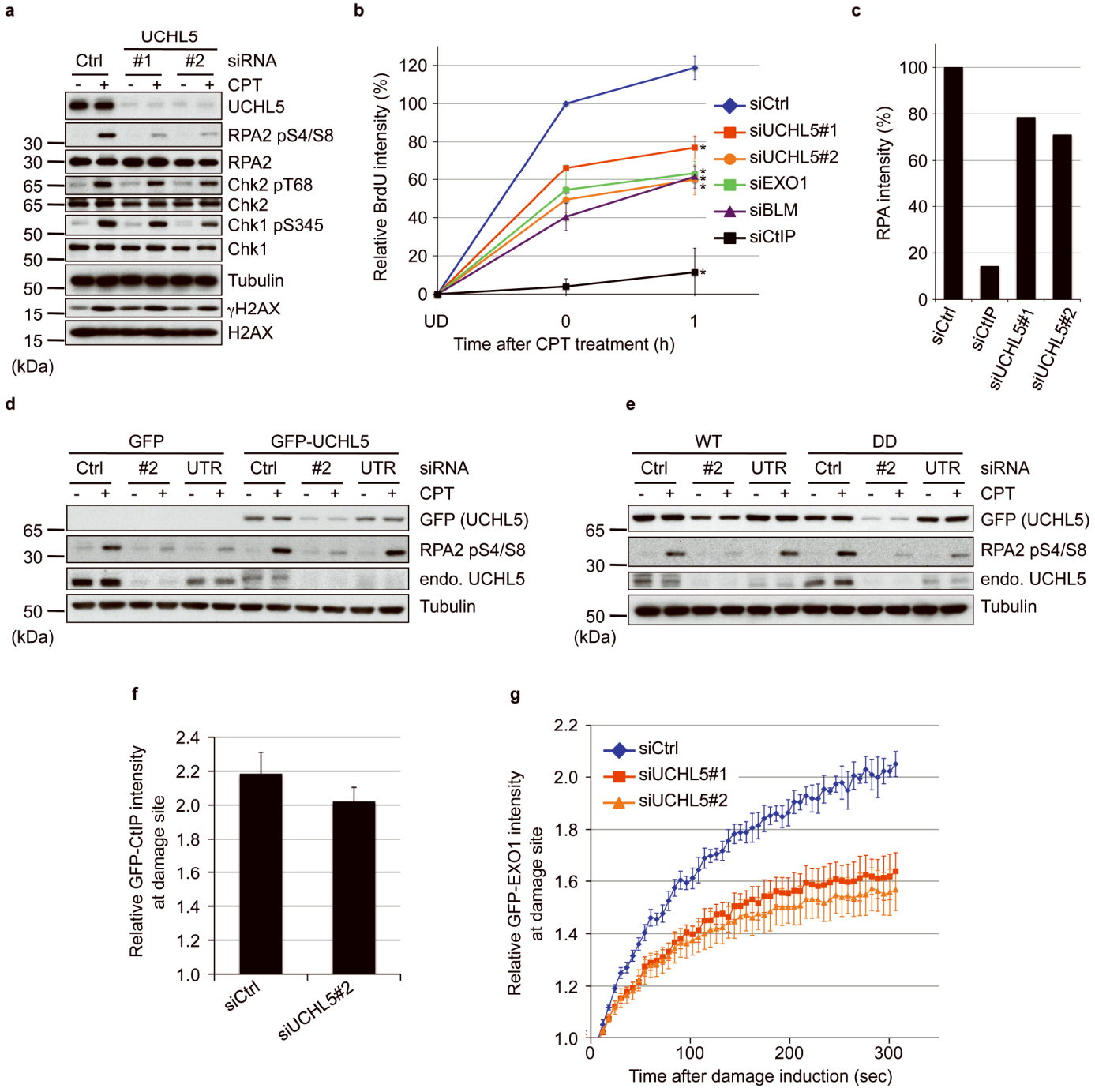
a
UCHL5
Ctrl
#1
#2
siRNA
CPT
UCHL5
RPA2 pS4/S8
RPA2
Chk2 pT68
Chk2
Chk1 pS345
Chk1
Tubulin
γH2AX
H2AX
30
30
65
65
50
50
50
15
15
(kDa)
b
Relative BrdU intensity (%)
120
100
80
60
40
20
0
UD
0
1
Time after CPT treatment (h)
siCtrl
siUCHL5#1
siUCHL5#2
siEXO1
siBLM
siCtIP
c
RPA intensity (%)
100
80
60
40
20
0
siCtrl
siCtIP
siUCHL5#1
siUCHL5#2
d
GFP
GFP-UCHL5
Ctrl
#2
UTR
Ctrl
#2
UTR
siRNA
CPT
GFP (UCHL5)
RPA2 pS4/S8
endo. UCHL5
Tubulin
65
30
50
(kDa)
e
WT
DD
Ctrl
#2
UTR
Ctrl
#2
UTR
siRNA
CPT
GFP (UCHL5)
RPA2 pS4/S8
endo. UCHL5
Tubulin
65
30
50
(kDa)
f
Relative GFP-CtIP intensity at damage site
2.4
2.2
2.0
1.8
1.6
1.4
1.2
1.0
siCtrl
siUCHL5#2
g
Relative GFP-EXO1 intensity at damage site
2.2
2.0
1.8
1.6
1.4
1.2
1.0
0
100
200
300
Time after damage induction (sec)
siCtrl
siUCHL5#1
siUCHL5#2

Figure 7

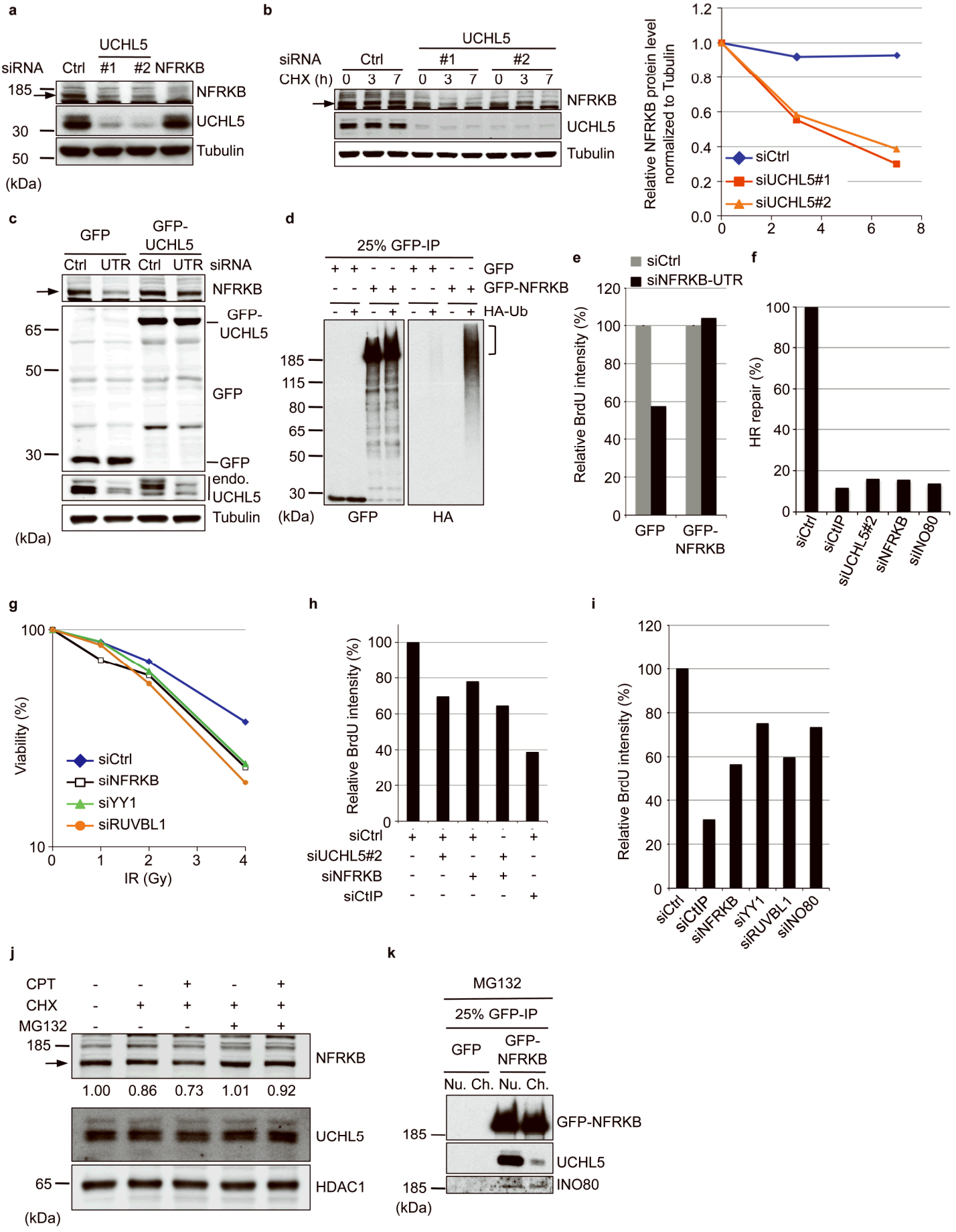
a
UCHL5
siRNA Ctrl #1 #2 NFRKB
185
30
50
NFRKB
UCHL5
Tubulin
(kDa)
b
UCHL5
siRNA Ctrl #1 #2
CHX (h) 0 3 7 0 3 7 0 3 7
NFRKB
UCHL5
Tubulin
Relative NFRKB protein level normalized to Tubulin
siCtrl
siUCHL5#1
siUCHL5#2
c
GFP
GFP-UCHL5
Ctrl UTR Ctrl UTR siRNA
NFRKB
GFP-UCHL5
GFP
GFP
endo. UCHL5
Tubulin
65
50
30
(kDa)
d
25% GFP-IP
GFP
GFP-NFRKB
HA-Ub
185
115
80
65
50
30
(kDa)
GFP
HA
e
siCtrl
siNFRKB-UTR
Relative BrdU intensity (%)
GFP
GFP-NFRKB
f
HR repair (%)
siCtrl
siCtIP
siUCHL5#2
siNFRKB
siINO80
g
Viability (%)
siCtrl
siNFRKB
siYY1
siRUVBL1
IR (Gy)
h
Relative BrdU intensity (%)
siCtrl
siUCHL5#2
siNFRKB
siCtIP
i
Relative BrdU intensity (%)
siCtrl
siCtIP
siNFRKB
siYY1
siRUVBL1
siINO80
j
CPT
CHX
MG132
185
NFRKB
1.00 0.86 0.73 1.01 0.92
UCHL5
65
HDAC1
(kDa)
k
MG132
25% GFP-IP
GFP
GFP-NFRKB
Nu. Ch. Nu. Ch.
185
GFP-NFRKB
UCHL5
185
INO80
(kDa)